広島大学学術情報リポジトリ
Hiroshima University Institutional Repository

Title	Design methodology using topology optimization for anti-vibration reinforcement of generators in a ship’s engine room
Author(s)	Daifuku, Masafumi; Nishizu, Takafumi; Takezawa, Akihiro; Kitamura, Mitsuru; Terashita, H.; Ohtsuki, Y.
Citation	Proceedings of the Institution of Mechanical Engineers, Part M: Journal of Engineering for the Maritime Environment , 230 (1) : 216 - 226
Issue Date	2014-07-25
DOI	10.1177/1475090214543081
Self DOI	
URL	https://ir.lib.hiroshima-u.ac.jp/00038754
Right	Authors
Relation	

Hiroshima University Institutional Repository

Design methodology using topology optimization for anti-vibration reinforcement of generators in a ship's engine room

Masafumi Daifuku [*] Takafumi Nishizu[*] Akihiro Takezawa [†‡] M. Kitamura[†]

H. Terashita [§] Y. Ohtsuki[§]

June 20, 2014

Abstract

Structural optimization for reinforcing the anti-vibration characteristics of the generators in the engine room of a ship, is presented. To improve the vibration characteristics of the structures, topology optimization methods can be effective because they can optimize the fundamental characteristics of the structure with their ability to change the topology of the target structure. Topology optimization is used to improve the characteristics of the anti-vibration reinforcement of the generators in the engine room. First, an experimentally observed vibration phenomenon is simulated using the finite element method for frequency response problems. Next, the objective function used in topology optimization is set as the dynamic work done by the load based on the energy equilibrium of the structural vibration. The optimization problem is then constructed by adding the volume constraint. Finally, based on finite element analysis and the optimization problem, topology optimization is performed on several vibration cases to improve their performance and reduce weight.

[*]Department of Transportation and Environmental Engineering Graduate School of Engineering, Hiroshima University, Japan
[†]Division of Mechanical Systems and Applied Mechanics, Institute of Engineering, Hiroshima University, Japan
[‡]Corresponding author, 1-4-1 Kagamiyama, Higashi-hiroshima, Hiroshima 739-8527, Japan. Email:akihiro@hiroshima-u.ac.jp
[§]Tsuneishi Shipbuilding Co., Ltd., Japan

1 Introduction

Anti-vibration characteristics are one of the most important design factors in the structure of ships. A ship experiences various serious vibrations during its operation, from the sea waves outside to internal sources such as the main engine or generators. The most important issue is to prevent serious damage by avoiding resonance of the ship's hull in a bending mode oscillated by external waves. In addition, resonance resulting from vibrations in the engine room can create an unpleasant environment for the crews. Details on this can be found in comprehensive textbooks [1, 2].

Historically, various methods have been proposed for analyzing the bending vibration of ships' hulls using basic mechanics such as beam theory [1, 2]. Subsequently, with the development of computer technology, the finite element method [3, 4] was introduced to the vibration analysis of the structure of a ship. Initially, approximation techniques for a ship's structure in vibration analysis were used because of the performance limits of computers [5, 6, 7]. However, recent developments in computer performance enable us to perform comprehensive computation of the vibration of the ship's structure using a detailed structural model [8, 9].

Moreover, in the development of technology for simulating a ship's performance, including vibration analysis, some optimization techniques were introduced into the design of ships using these simulation results. This topic was studied in various fields related to ship building such as hull form design for hydrodynamic performance [10, 11], multidisciplinary objectives [12] and fresh water tank design to avoid local resonance of the hull [13]. Structural static design is also an important topic in design optimization, for example, the optimization of a partial mid-ship structure by Rahman and Caldwell [14], Kitamura and Uedera [15] and Kitamura et. al. [16], and the optimization of panel and girder designs by Rahman [17, 18, 19]. In the context of anti-vibration design, the optimization of the plate thickness of a ship's hull around the engine room has been reported [8].

Structural optimization techniques used in this research are classified into the following three categories: size, shape and topology optimization. Of these, topology optimization [20, 21, 22] can optimize the fundamental characteristics of the structure because of its ability to change the topology (number of holes) of the target structure. However, in the context of marine structures, little research has been reported. Rais-Rohani

and Likits developed a layout design methodology for reinforcing submarine structures based on topology optimization [23].

In this research, we optimize the reinforcing shape of the engine room using topology optimization to improve anti-vibration characteristics in bulk cargo ships. Generators, as well as the main engine, can be serious vibration sources. Thus, their supporting structures have an important role in creating a good environment for the ship's crew. This research is performed using the following processes. First, an experimentally-observed vibration phenomenon is simulated using the finite element method for frequency response problems. Next, the objective function used in the topology optimization is set as the norm of the amplitude vector, corresponding to the load input points, and approximately representing the dynamic work done by the load. The optimization problem is then constructed by adding the volume constraint. Based on finite element analysis and the optimization problem, topology optimization is performed for several types of vibration conditions using the commercial software, Optistruct (Altair Engineering, Inc., Troy, Michigan, USA.). Finally, by comparing the optimized results with the original results, the validity and utility of the proposed methodology were confirmed.

2 Design target

In this research, we intend to generate optimal reinforcement of the generators to reduce their vibrations. Generators can cause relatively higher frequency vibrations than the main engine. The design optimization is performed based on the actual structure of a ship using the vibration experimental data. The target ship is a G.T. 92,900 t bulk carrier and its generators have a 675 kW output with five cylinders. The generators are located on the third deck in the engine room. They were mounted to the deck without anti-vibrating supports such as flexible bushes. The model for the part used in this research is shown in Fig. 1. Mechanisms for the generators' vibrations are the vibration of the base plate by the vertical periodic force created by the crank movement of the diesel engine driving the generator. We define the vibration reduction problem as the minimization of the amplitude of the plate vibrations around the generators. Because the direct way to suppress the vibration of generators is to strengthen their supporting structure, excess reinforcements are

placed under the third deck, in the current design, to reduce the vibration. The bottom reinforcement is usually composed of several transverses and girders.

Because the model shown in Fig. 1 was based on an actual ship, several details of the structure have been omitted for confidentiality reasons. The structure modeled only part of the 3rd deck supporting the generators when performing the detailed vibration analysis around the generators. Because the actual structure was surrounded by the inner hull plates, the stiffness contribution of the surrounding structure to the current model was modelled as the ground spring. This implementation of the ground spring element is performed by adding the spring rate value to the stiffness matrix of the parts corresponding to the nodes at the boundary between the current model and the surrounding structure [24]. The size of the model was about L:7200×W:11200×H:5500 mm as the maximum length in each axis. The model was composed of nine floors and seven girders. The thicknesses of the transverses and girders were 12 and 9 mm. The base plate of the 3rd deck was 20 mm. Several stiffeners were also included in the model. The total weights of the whole model and the design target structures shown in Fig. 1 were about 46 and 13.5 t excluding the weights of the generators.

The size of the placement plane and weight of the generators were about L:3600×W:850 mm and 14380 kg. The generators were handled as non-structural masses in the model. The weights of the generators were distributed over their placement areas. The generators were numbered 1-3 as shown in Fig. 1.

The bottom reinforcement of the structure was set as the design target in this research. The detailed shapes are shown in Fig. 1. The transverses were numbered T1 to T7 from stern to bow. The girders were numbered G1 to G6 from right to left.

3 Vibration analysis

3.1 Equation for the steady state response

The vibration propagation from the generator can be regarded as a steady state propagation of a sinusoidal periodic force. That is, this phenomenon is solved as a frequency response problem of the ship's structure as

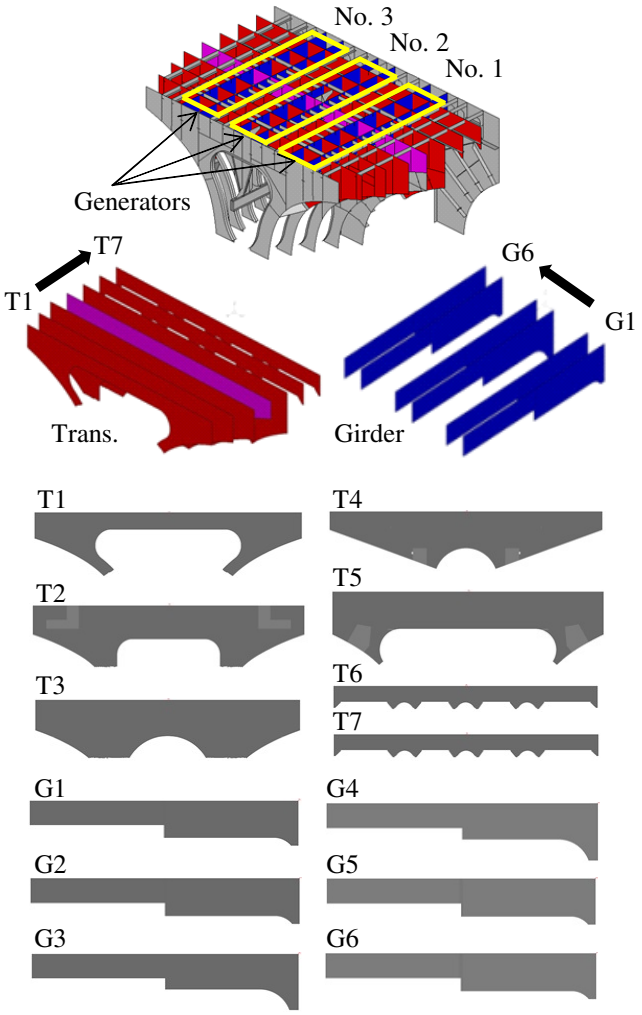

Figure 1: Outline of the analysis and design target model.

a function of the periodic load from the generator. The calculations for the problem were performed using the Finite Element Method (FEM). The discretized form for the vibration equation of the structure under a periodic load is represented as follows:

$$(\mathbf{K} - \omega^2 \mathbf{M})\mathbf{u} = \mathbf{F} \tag{1}$$

where $\mathbf{K}$ and $\mathbf{M}$ are the stiffness and mass matrices, $\mathbf{u}$ and $\mathbf{F}$ are the amplitude and load vectors and ω is the angular frequency of the input load.

3.2 Vibration measurement and analysis results for the original structure

First, the experimental data for the vibration around the generator were reviewed. The vibration from the generator was dominated by 30 Hz oscillations corresponding to the second order vibration of the generator crank. The vertical vibration was measured at six points on the deck around each generator using uni-axis accelerometers. The measurements were performed when the ship was in harbor and the main engine was stopped. As vibration cases, the following six patterns were considered: Cases 1-3, generators No.1, 2 or 3 working singly; Case 4, generators No.1 and 2 both working; Case 5, generators No.1 and 3 both working; Case 6, generators No.2 and 3 both working. Figure 2 shows the averaged acceleration amplitudes at the measurement points for each generator as black bars. For confidentiality reasons, normalized values based on the average values are used in this paper.

Vibration analysis was then performed for the normal structure. The FEM model was constructed based on the structure shown in Fig. 1 using 170,010 first order 4 node quad shell elements. The total degrees of freedom of the model is 974,292. Several parameters for the vibration simulation were set based on the vibration test. The periodic load applied to the base plate from the generator can be regarded as the inertia force of the generator. This value was calculated as 9000 N by multiplying the weight and the measured acceleration of the generator. This load was applied to the model as a sinusoidal distributed load with the same phase on the placement plane. The frequency of the periodic load was set to 30 Hz which corresponded to the second order vibration of the five cylinder generator. The same points were used as the evaluation points in the numerical analysis. The ground spring values set at the points corresponding to the welding

points of the ship's shell were adjusted to match the analysis results to the experimental results. All FEM calculations were performed using Optistruct (Altair Engineering, Inc., Troy, Michigan, USA.). Analysis results are shown in Fig. 2 using the gray bars. The normalized acceleration amplitude values were also used in the analysis results.

Although, strict matched results were not obtained, the vibration propagation from the source generator to the other generators was simulated, except for Case 5. In the experimental data of the Case 5 vibration, the vibrations from No. 1 and 3 generators seemed to be blocked by No.2 generator. In the actual ship, No. 2 generator may have strong support behind it. However, in our modeling, because the constant spring rate was set around the analysis model, such local strong support could not be represented. Considering the simplicity and the good matching in the other five cases, we accept this analysis model for the optimization study. The average errors between the experimental and numerical results in each case were about 10% except for Case 5. We performed the optimization under the assumption that if the vibration performance of the analysis model was improved to a certain level, the performance of the actual ship was also improved at the same rate on average, although both have about 10% errors.

Figure 3 shows the deformed structure in each vibration case, and all vibration shapes have one anti-node on the third deck plate. Thus, all vibrations of the third deck plate may be dominated by the first order vibration. The frequency response performance was also checked because if the eigen frequency was close to the input vibration frequency, the optimization could be unstable. Figure 4 shows the average amplitude at the vibration input points obtained by varying the input frequency from 0 to 60 Hz. In all vibration cases, the dominant vibration frequency, 30 Hz, was adequate for the resonance frequencies. Thus, stable optimization should be achievable.

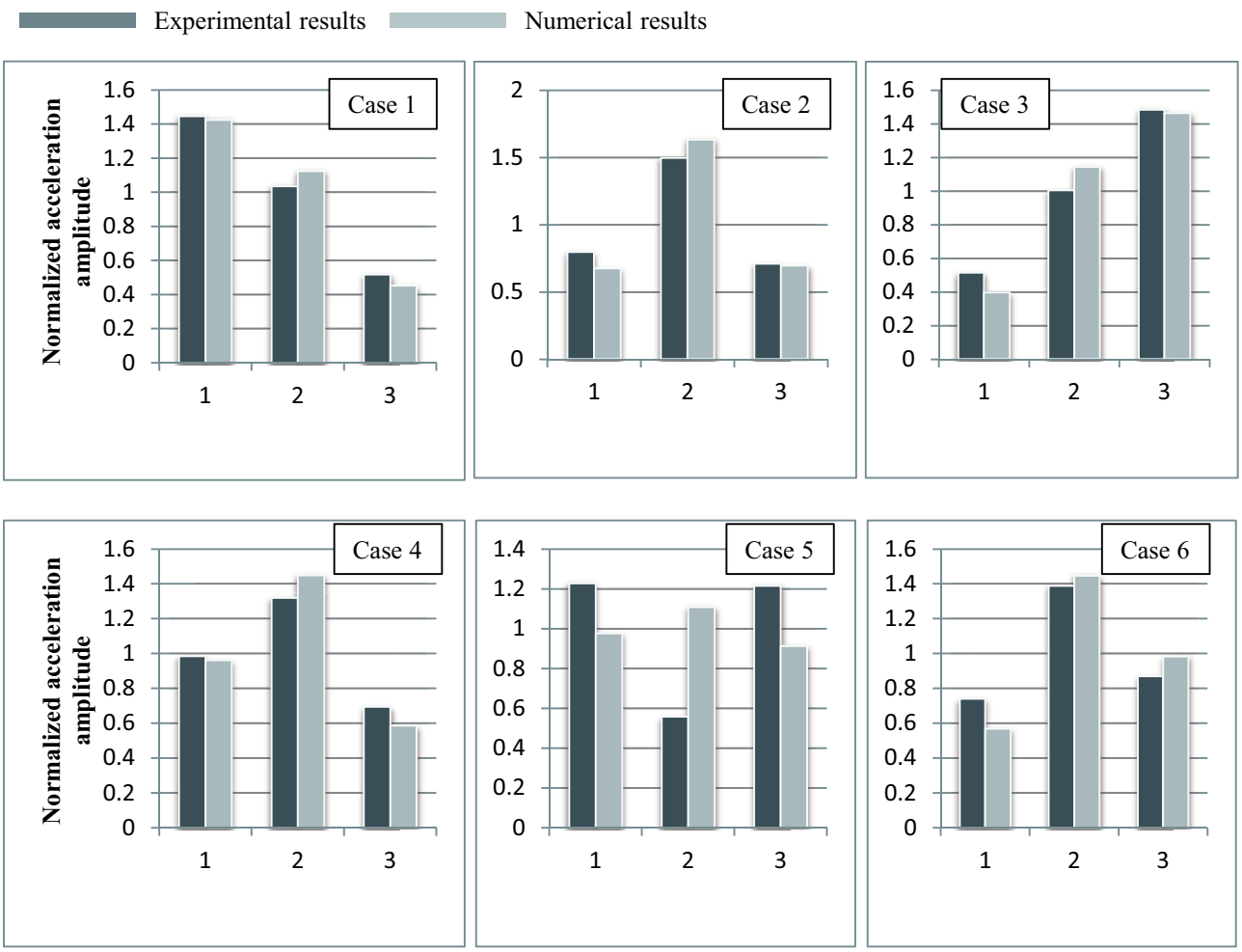

Figure 2: Comparison between vibration measurements and analysis results. Cases 1-3, generator No.1, 2 or 3 working singly; Case 4, generators No.1 and 2 both working; Case 5, generators No.1 and 3 both working; Case 6, generators No.2 and 3 both working.

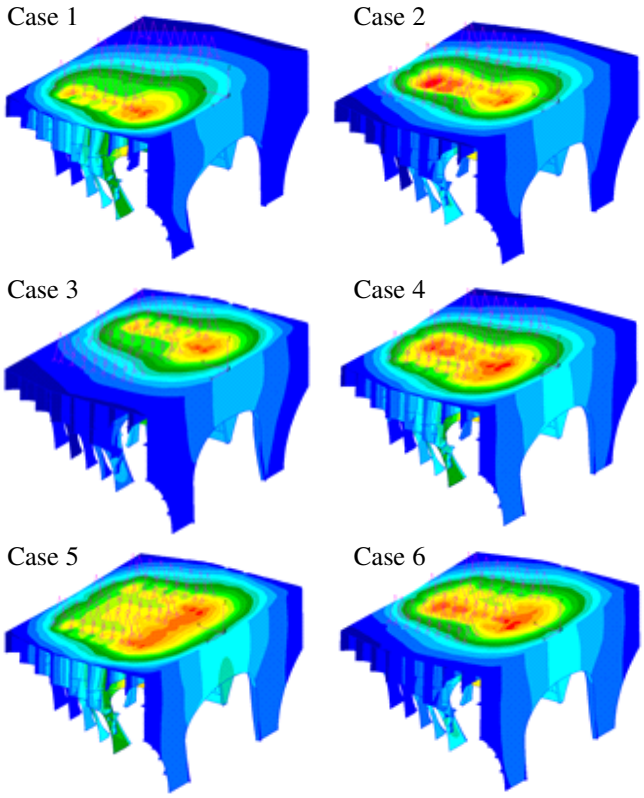

Figure 3: Deformation shapes of the 3rd deck. Red indicates large deformation.

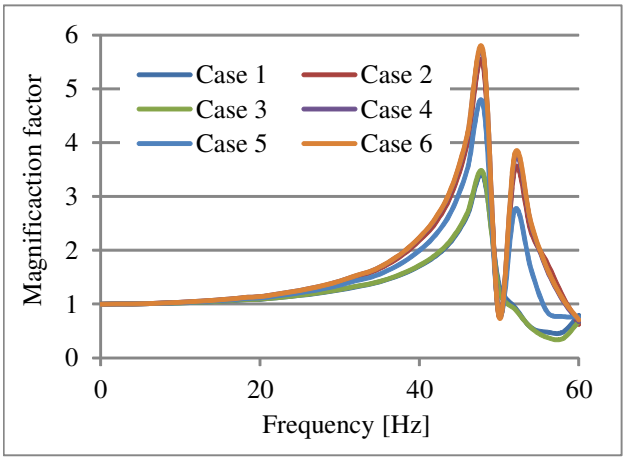

Figure 4: Vibration measurement and analysis results. Cases 1-3, generator No.1, 2 or 3 working singly; Case 4, generators No.1 and 2 both working; Case 5, generators No.1 and 3 both working; Case 6, generators No.2 and 3 both working.

4 Topology optimization

4.1 Interpolation Method

Topology optimization was used as the geometrical optimization method for the anti-vibration reinforcement of the generators, because this method can perform fundamental optimizations including shape and topology; *viz.*, the number of holes. The fundamental concept was to introduce a fixed, extended design domain D that included *a priori* the optimal shape Ω_{opt}, that is, $\Omega_{\text{opt}} \subset D$, and used the characteristic function:

$$\chi(\mathbf{x}) = \begin{cases} 1 & \text{if} \quad \mathbf{x} \text{ in } \Omega_{\text{opt}} \\ 0 & \text{if} \quad \mathbf{x} \text{ not in } \Omega_{\text{opt}} \end{cases} \tag{2}$$

The original design problem for the target shape is replaced by a material distribution problem incorporating a physical property, χA, in the extended design domain D, where A is an arbitrary physical property of the original material of the target shape. In this problem, A is Young's modulus and mass density. In short, the optimal shape Ω_{opt} is represented as the set of $\mathbf{x}$ satisfying $\chi(\mathbf{x}) = 1$. Unfortunately, the optimization problem did not have any optimal solutions. One way to address this problem is to introduce a homogenization method [20, 21]. Through this process, the original material distribution optimization problem with respect to the characteristic function was replaced by an optimization problem of a "composite" composed of the original material and a material with very low physical properties that mimic voids with respect to the density function. This density function represented a fraction of the volume of the original material. In this procedure, the relationship between the material properties of the "composite" and the density function must be defined. The Solid Isotropic Material with Penalization (SIMP) method is the most popular approach, which sets a penalized proportional material property [25, 22]. The basic idea of SIMP is to use a fictitious isotropic material whose Young's modulus E and mass density ρ are assumed to be a function of the penalized material density d as follows:

$$E^* = d^3 E_{\text{o}}, \tag{3}$$

$$\rho^* = d\rho, \tag{4}$$

with

$$0 \leq d(\mathbf{x}) \leq 1, \tag{5}$$

where the upper asterisk represents the interpolated value of the physical properties.

4.2 Optimization Problem

The aim of this study was to generate a structure with anti-vibration characteristics. We regarded the vibration suppression as a reduction in the acceleration amplitude vector in the frequency response problem represented in Eq. (1) around the base plate of the generators. According to the deformation shapes of the vibrations shown in Fig. 3, because the vibration was dominated by the first mode, the amplitude reduction for the whole structure should have been effective for our purpose. For such a design objective, the dynamic compliance which was equal to double the sum of the kinetic and strain energies was proposed by Ma et.al. [26] as follows:

$$\mathbf{F}^T\mathbf{x} = \ddot{\mathbf{x}}^T\mathbf{M}\ddot{\mathbf{x}} + \mathbf{x}^T\mathbf{K}\mathbf{x} \tag{6}$$

where $\mathbf{x}$ is the displacement vector. The above equation was obtained by multiplying the usual dynamic equation $\mathbf{M}\ddot{\mathbf{x}} + \mathbf{K}\mathbf{x}$ by $\mathbf{x}^T\mathrm{d}t$ and integrating with respect to t.

In the usual topology optimization, dynamic compliance has the advantage that the adjoint equation does not need to be calculated because it is a self adjoint function in terms of sensitivity analysis. Unfortunately, this dynamic compliance cannot be handled as the objective function in topology optimization using the commercial software Optistruct which was used in this research. Thus, the objective function was replaced as the norm of the amplitude vector at the loading points. Because the force vector $\mathbf{F}$ had non-zero values only at the components corresponding to the loading points, if the load values were constant at every loading point, the minimization of the square of the norm of the amplitude vector could directly lead to the minimization of the dynamic compliance. By introducing a volume constraint, the optimization problem was formulated as follows:

$$\text{Minimize } ||\mathbf{u}_{\text{input}}(\mathbf{d})||^2 = \mathbf{u}_{\text{input}}^T\mathbf{u}_{\text{input}} \tag{7}$$

Subject to

Eq. (1)

$$V(\mathbf{d}) \leq V_{\max} \tag{8}$$

$$0 \leq d_i \leq 1 \text{ in } \mathbf{d} = [d_1, ..., d_n] \tag{9}$$

where $\mathbf{u}_{\text{input}}$ is the local amplitude vector corresponding to the loading points, V and $V_{\max}$ are total volumes of the designed structure and its maximum value respectively and $\mathbf{d}$ is the design variable vector.

4.3 Algorithm

The optimization was performed using an algorithm incorporating the sensitivity calculation and updating the design variable using the Convex Linearization Method (CONLIN) [27]. The optimization algorithm is presented in Fig. 5.

The sensitivity of the local amplitude norm with respect to i-th design variable d_i is calculated as follows:

$$\frac{\partial \mathbf{u}_{\text{input}}^T \mathbf{u}_{\text{input}}}{\partial d_i} = -\tilde{\mathbf{u}}^T \left(\frac{\partial \mathbf{K}}{\partial d_i} - \omega^2 \frac{\partial \mathbf{M}}{\partial d_i} \right) \mathbf{u} \tag{10}$$

where

$$\mathbf{u}_{\text{input}} = \mathbf{H}\mathbf{u} \tag{11}$$

$$2\mathbf{u}^T \mathbf{H}^T \mathbf{H} - \tilde{\mathbf{u}}^T (\mathbf{K} - \omega^2 \mathbf{M}) = 0 \tag{12}$$

and $\mathbf{H}$ is an index matrix determining the local amplitude vector at the loading points from the global amplitude vector and $\tilde{\mathbf{u}}$ is an adjoint variable. The detailed derivation of these equations is shown in the Appendix.

5 Optimization studies

Topology optimization is performed for the target structure shown in Fig. 1. The bottom reinforcements of the structure shown in Fig. 1 are set as the design domain for the Topology optimization. The volume

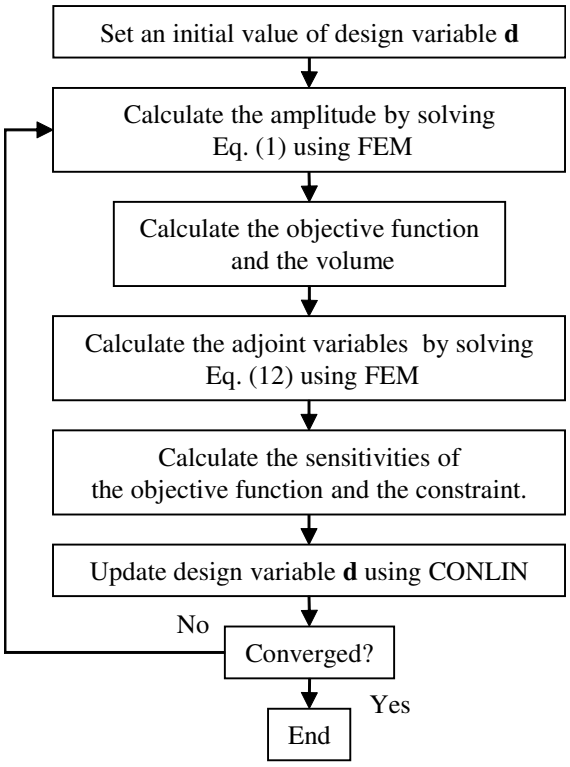

Figure 5: Flow chart of the optimization algorithm.

constraint is set based on the maximum total volume obtained by multiplying the area of the design domain parts by their thickness. The convergence criterion is set to be when the variation rate of the objective function becomes less than 10^{-6}.

5.1 Optimization for each vibration case

To confirm the validity of the proposed optimization, it was performed for each vibration case identified in Fig. 2. The volume constraint was set to 60% of the original volume of the reinforcement parts. However, the maximum thickness of the plate was set to 5/3 times the original thickness. Thus, 60% of the volume of the design domain corresponded to the total volume of the design domain with the original thickness. According to these settings, we were able to confirm the performance improvement from the original design by the optimization for the same volume.

Optimizations were performed for each of the six vibration cases. We first focused on the optimization for

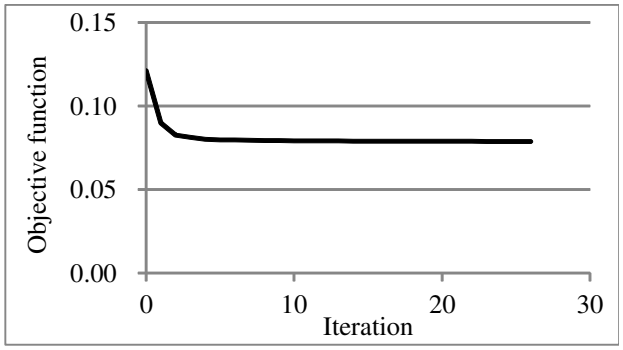

Figure 6: Convergence history for the topology optimization of the vibration Case 1 in which only No. 1 generator was working.

Table 1: Rate of increase of the norm of the average acceleration amplitude vector at the location of each generator and its average value by optimization for each case [%]. Negative values indicate vibration reduction.

	Measuring points (No. of generators)			
	No. 1	No. 2	No. 3	Average
Vibration cases				
Case 1	-13.6	-34.3	-83.8	-26.6
Case 2	-35.7	-25.4	-35.9	-29.5
Case 3	-83.7	-34.5	-15.3	-27.5
Case 4	-22.6	-27.6	-45.7	-28.8
Case 5	-24.0	-34.6	-24.0	-27.6
Case 6	-45.7	-27.7	-22.8	-28.8

vibration Case 1. Figure 6 shows the convergence history of the objective function. A smooth reduction of the objective function was observed until the convergence at the 26th iteration. Figure 7 shows the optimal configurations. Both the outline and the detailed shape of each reinforcement are shown. The reinforcements were concentrated under the working generators. Table 1 shows the performance improvement calculated as the rate of increase of the norm of the average acceleration amplitude vector at the location of each generator and its average value. Acceleration amplitudes were reduced in all cases and the vibration performances were improved. The optimization results for the other vibration cases are also outlined Fig. 7 and Table 1. We confirmed the optimization worked well for all the vibration cases.

5.2 Optimization for a general vibration case

Because the optimizations were performed for each case in the previous example, the optimal results obtained cannot be used as an actual ship's structure. In the actual running of the ship, working generators were

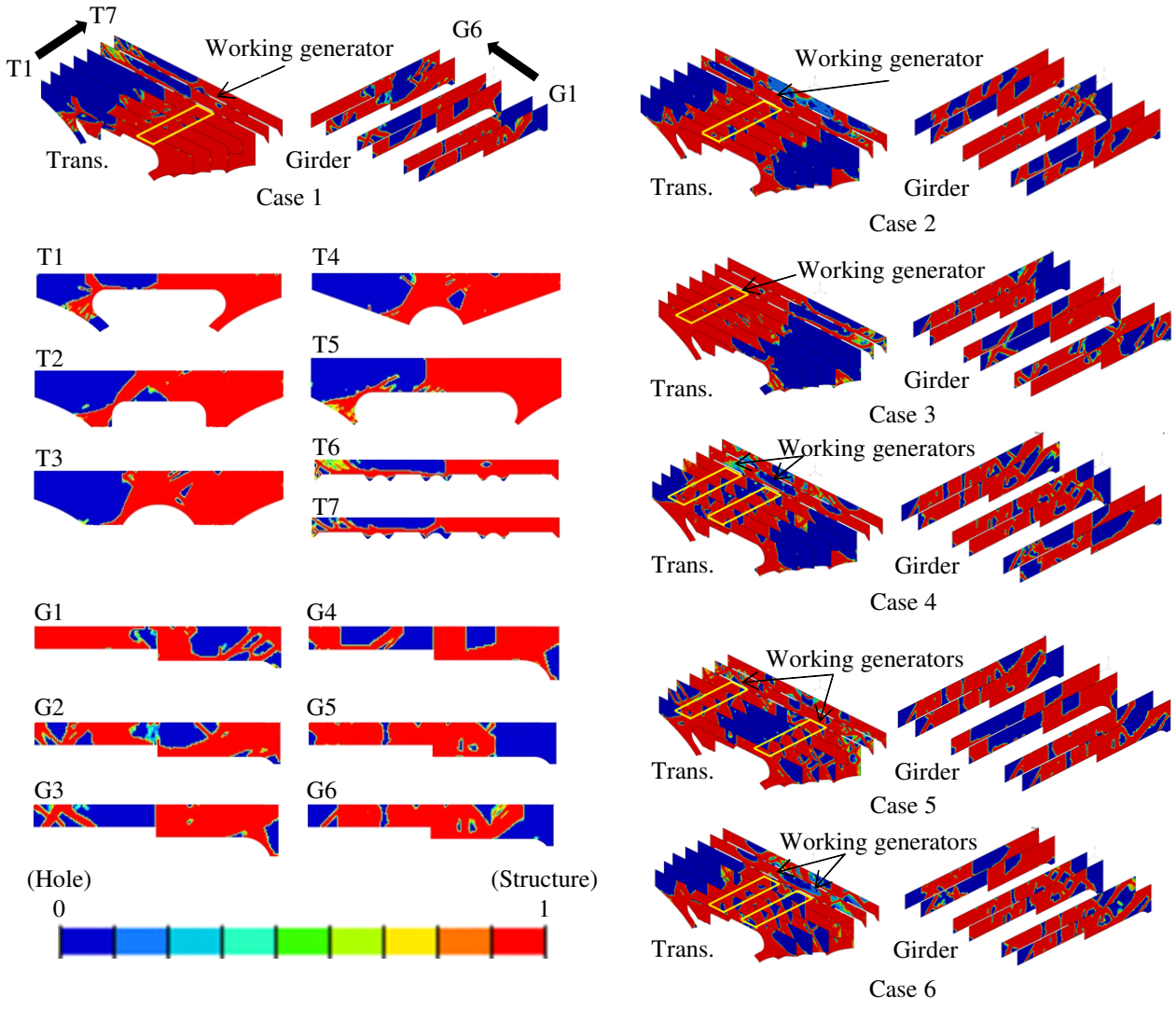

Figure 7: Optimal configurations obtained by topology optimization for each vibration case. Cases 1-3, generator No.1, 2 or 3 working singly; Case 4, generators No.1 and 2 both working; Case 5, generators No.1 and 3 both working; Case 6, generators No.2 and 3 both working. The red color represents the steel structure and the blue color represents a hole as shown in the colorbar. Detailed shapes for the optimal reinforcement are shown only for the results of Case 1.

changed and we could not specify which for any specific case. During the voyage, any one or two generators work according to conditions, by rotation. In other words, all cases must be considered in the optimization. The straightforward way for handling different vibration conditions in one optimization problem is to integrate all conditions using the weighting coefficient method. However, this approach results in large computational cost for six finite element analyses in each of the optimization iterations and can lead to poor convergence. Consequently, we introduced the vibration case for all of them working simultaneously as a general case considering all the generators. The periodic forces were applied to every generator and the objective function was set as the norm of the amplitude vector corresponding to all the generators, which has the same physical meaning as the dynamic work done by the load of all the generators. The plate thicknesses were set to be the same as in the previous example. We performed optimizations under 60%, 55% and 50% volume constraints. Because the 60% volume constraint corresponded to the original weight, the 55 and 50% volume constraints represented generating designs within $55/60 = 92$[%] and $50/60 = 83$[%] of the original weight. About $13.5 \times 0.08 = 1.1$ t and $13.5 \times 0.08 = 2.3$ t weight reduction was achieved through these optimizations.

Figure 8 shows the optimal configurations. Supports were applied under all the generators. The side and center part of large transverses T1-T5 were removed for weight reduction. Because the direction of vibration of the generators was vertical, side supports did not seem to be important. Moreover, the transverses T6 and T7 were almost removed except for the side parts. This means the T6 and T7 parts were excessive for vibration suppression because they were outside the location of the generators. In the case of the girders, the back parts were removed because, similar to transverses T6 and T7, they were outside the location of the generators. Table 2 shows the performance improvement calculated as the increased rate of the norm of the average acceleration amplitude vector at the location of each generator, and their average value when Cases 1-6 vibrations were applied to the optimal result. In the results for the 60% volume constraint, because the reduction of the averaged amplitude was confirmed in all the vibration cases, this optimization configuration was as valid as the general configuration. In the 55% volume constraint optimization, although the vibration increased for some of the generator positions, the average vibrations were reduced for all the vibration cases. Thus about a 5% performance improvement was achieved together with about a 1.1 t weight reduction in

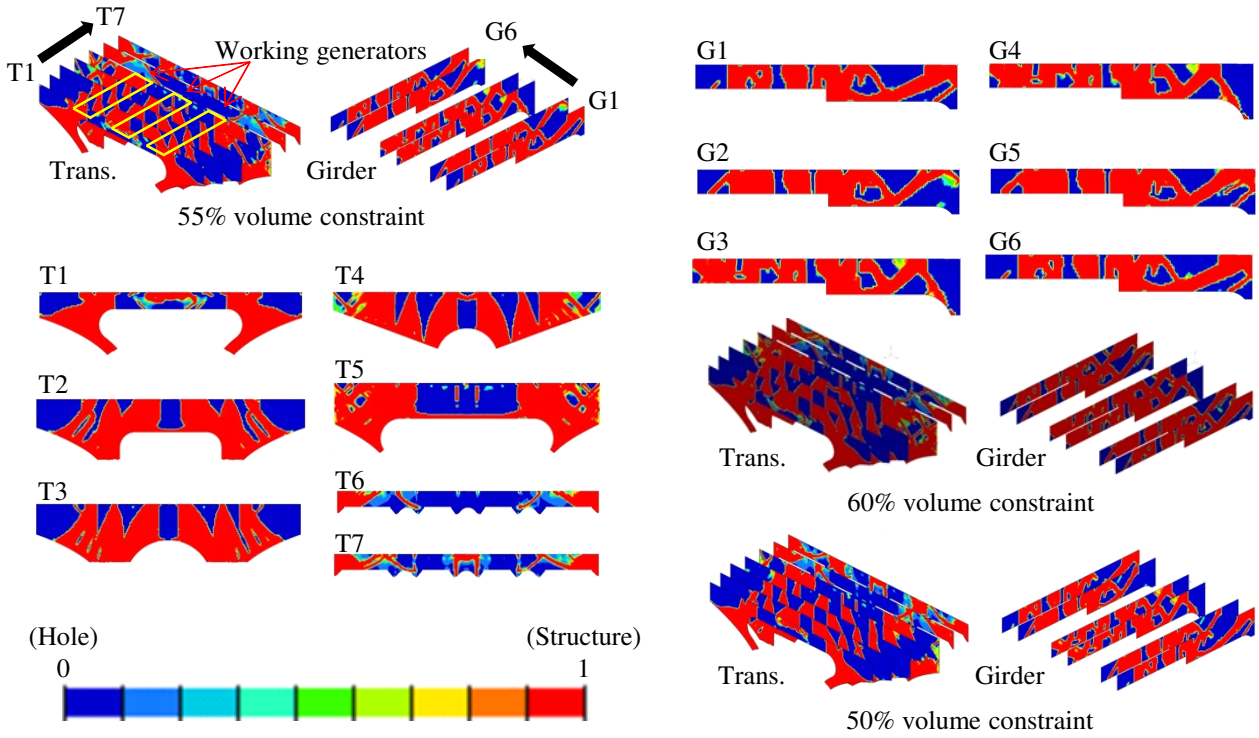

Figure 8: Optimal configurations obtained by topology optimization for the general vibration case which assumed all generators were working simultaneously. Detailed shapes of the optimal reinforcement are shown only for the 55% volume constraint results.

this example. In the 50% volume constraint optimization, vibrations reduced and increased by about half in each case and the averaged vibration was almost equal to the original structure. That is, 2.3 t weight reduction was achieved while maintaining an average vibration performance.

5.3 Optimization for weight reduction with minimum performance reduction

In the previous example, we used thicker plates than the original to emphasize the optimization effect. However, when the increase in the plate thickness was not allowable, these optimal configurations could not be used as an actual design. We then studied the weight reduction problem using the same thickness plates as the original design. Because the structural stiffness performs a more important role for the vibration performance than the structural mass in a 30 Hz low frequency vibration, the weight reduction of the structure with the same thickness plate could lead to a reduction in performance. However, this can be minimized

Table 2: Rate of increase of the norm of the average acceleration amplitude vector at the location of each generator and its average value by optimization under different volume constraints [%]. Negative values indicate vibration reduction.

		Measuring points (No. of generators)			
		No. 1	No. 2	No. 3	Average
Volume constraints	Vibration cases				
60%	Case 1	11.6	-19.3	-82.8	-8.4
	Case 2	-20.7	2.6	-20.6	-7.2
	Case 3	-82.7	-19.2	9.9	-9.13
	Case 4	-1.8	-3.3	-34.9	-8.1
	Case 5	-4.5	-19.5	-4.1	-9.5
	Case 6	-35.3	-3.4	-1.5	-8.0
55%	Case 1	15.0	-17.4	-87.4	-6.3
	Case 2	-19.7	8.4	-19.4	-3.4
	Case 3	-87.3	-17.3	15.2	-6.0
	Case 4	2.1	1.23	-35.8	-4.8
	Case 5	-1.2	-18.5	-0.8	-6.9
	Case 6	-36.3	1.0	2.2	-4.8
50%	Case 1	20.9	-13.2	-89.0	-1.7
	Case 2	-18.0	14.9	-17.4	1.2
	Case 3	-88.9	-13.1	21.2	-1.3
	Case 4	-6.4	-6.5	-35.9	-0.8
	Case 5	2.7	-16.7	3.3	-3.7
	Case 6	-36.6	6.3	6.7	-0.7

through the optimization.

We performed optimizations by setting the volume constraint at 90, 80, 70 and 60% of the original structure. Table 3 shows the performance improvement calculated as the rate of the increase in the norm of the average acceleration amplitude vector at the location of all the generators when the vibrations of Cases 1-6 were applied to the optimal result. Figure 9 shows the optimization results for each volume constraint. The performance clearly decreased as the volume constraint became smaller. The 90% volume constraint results showed almost the same performance as the original results. This indicated that about 10% of the parts was wasted in the context of vibration reduction performance. Other results can be used for the weight reduction of the structure if the structure performance margin is over the criteria limit. For example, up to the 70% volume constraint, the performance reductions were within 10%. When the structural performance has a greater than 10% margin above the criteria limit, this method might be useful for designing a weight reduction of up to 70% of the weight of the original design.

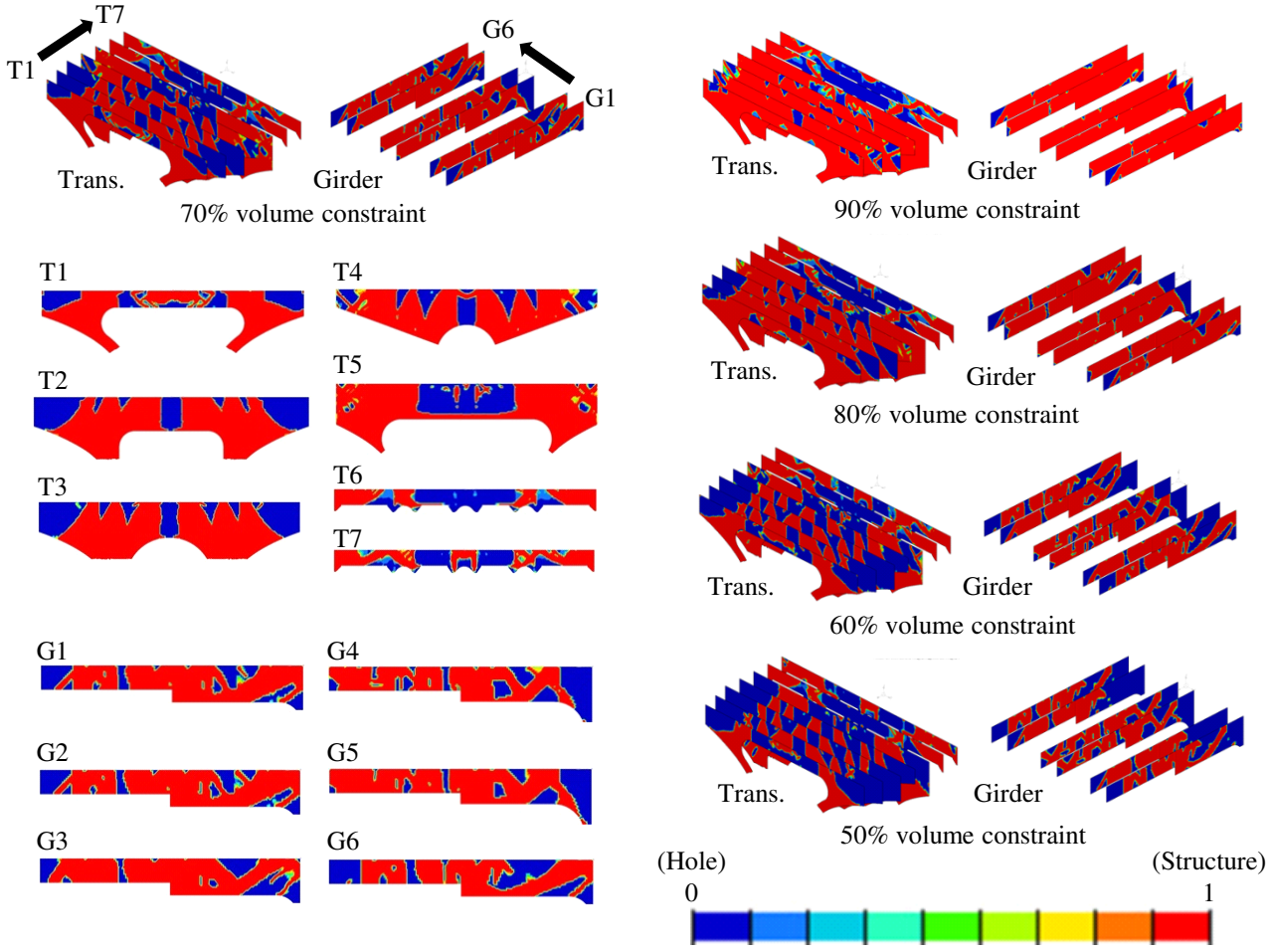

Figure 9: Optimal configurations obtained by topology optimization with the original plate thickness for the general vibration case. Detailed shapes of optimal reinforcement are shown only for the 70% volume constraint results.

Table 3: Rate of increase of the norm of the average acceleration amplitude vector at the location of all the generators by optimization for different volume constraints [%]. Negative values indicate vibration reduction.

	Vibration cases					
	Case 1	Case 2	Case 3	Case 4	Case 5	Case 6
Volume constraints						
90%	0.0	1.1	0.0	0.7	0.0	0.6
80%	1.1	3.7	1.6	3.1	1.3	1.4
70%	4.4	9.2	5.1	7.2	4.3	7.4
60%	13.0	18.0	14.2	14.0	9.6	14.3
50%	28.2	28.2	30.0	24.2	18.4	24.7

6 Conclusions

In this research, we optimized the reinforcement shape of the engine room using topology optimization to improve the anti-vibration characteristics. The details are as follows:

1. A generator vibration phenomenon observed experimentally was simulated with a small local model around the generators using the finite element method.

2. The objective function used in the topology optimization was set as the norm of the amplitude vector corresponding to the input force nodes, instead of the dynamic work done by the load.

3. Topology optimizations were performed for six vibration cases. The performance improvements were observed in each case.

4. The virtual vibration case for three generators working simultaneously was set as the Topology optimization for a general vibration case. Using 5/3 times the thickness of the original plates, a vibration reduction of about 8% was achievable. Moreover, by setting the volume constraint to more strict values, a 1.1 t weight reduction with a vibration reduction of about 5%, and a 2.3 t weight reduction maintaining the average vibration reduction was achievable.

5. Keeping the plate thickness at the original value, the optimizations were performed for pure weight reduction with minimum performance reduction. The relationship between the weight reduction and performance reduction was clarified.

Note that, any structural issues were not considered in the proposed vibration optimization. Although the structural stiffness could be increased in the optimization for an adequate range of lower frequencies than the first eigen frequency, other structural strength performance characteristics could be decreased through the optimization. Thus, these issues should be adequately studied in the re-design of the structure based on the optimization results.

acknowledgements

This work was supported by the JSPS KAKENHI Grant Numbers 24360356 and 25820422.

References

[1] Todd FH. Ship Hull Vibration. London: Edward Arnold Publishers; 1961.

[2] Rawson KJ, Tupper EC. Basic Ship Theory. Fifth edition ed. Oxford: Butterworth-Heinemann; 2001.

[3] Kamel HA, Liu D. Application of the finite element method to ship structures. Comput Struct. 1971;1(1):103–130.

[4] Kawai T. The application of finite element methods to ship structures. Comput Struct. 1973;3(5):1175–1194.

[5] Skaar KT, Carlsen CA. Modelling aspects for finite element analysis of ship vibration. Comput Struct. 1980;12(4):409–419.

[6] Senjanović I, Ying F. On modelling of thin-walled girders and accuracy of vibration analysis performed by the finite element technique related to ship structures. Comput Struct. 1990;34(4):603–614.

[7] Senjanović I, Grubisić R. Coupled horizontal and torsional vibration of a ship hull with large hatch openings. Comput Struct. 1991;41(2):213–226.

[8] Kong YM, Choi SH, Song JD, et al. OPTSHIP: a new optimization framework and its application to optimum design of ship structure. Struct Multidisc Optim. 2006;32(5):397–408.

[9] Lin TR, Pan J, O'Shea PJ, et al. A study of vibration and vibration control of ship structures. Mar Struct. 2009;22(4):730–743.

[10] Saha GK, Suzuki K, Kai H. Hydrodynamic optimization of ship hull forms in shallow water. J Mar Sci Technol. 2004;9(2):51–62.

[11] Tahara Y, Stern F, Himeno Y. Computational fluid dynamics-based optimization of a surface combatant. J Ship Res. 2004;48(4):273–287.

[12] Yang YS, Park CK, Lee KH, et al. A study on the preliminary ship design method using deterministic approach and probabilistic approach including hull form. Struct Multidisc Optim. 2007;33(6):529–539.

[13] Kong YM, Choi SH, Yang BS, et al. Development of integrated evolutionary optimization algorithm and its application to optimum design of ship structures. J Mar Sci Technol. 2008;22(7):1313–1322.

[14] Rahman MK, Caldwell JB. Rule-based optimization of midship structures. Mar Struct. 1992;5(6):467–490.

[15] Kitamura M, Uedera T. Optimization of ship structure based on zooming finite element analysis with sensitivities. Int J Offshore Polar Eng. 2003;13(1):60–65.

[16] Kitamura M, Hamada K, Takezawa A, et al. Shape Optimization System of Bottom Structure of Ship Incorporating Individual Mesh Subdivision and Multi-Point Constraint. Int J Offshore Polar Eng. 2011;21(3).

[17] Rahman MK. Multilevel optimization applied to hull girder design using three panel forms. Struct Optim. 1994;7(1):126–137.

[18] Rahman MK. Optimization of panel forms for improvement in ship structures. Struct Optim. 1996;11(3):195–212.

[19] Rahman MK. Automated optimization of transverse frame layouts for ships by elastic-plastic finite element analysis. Struct Optim. 1998;15(3):187–200.

[20] Bendsøe MP, Kikuchi N. Generating optimal topologies in structural design using a homogenization method. Comput Meth Appl Mech Eng. 1988;71(2):197–224.

[21] Suzuki K, Kikuchi N. A homogenization method for shape and topology optimization. Comput Meth Appl Mech Eng. 1991;93(3):291–318.

[22] Bendsøe MP, Sigmund O. Topology Optimization: Theory, Methods, and Applications. Berlin: Springer-Verlag; 2003.

[23] Rais-Rohani M, Lokits J. Reinforcement layout and sizing optimization of composite submarine sail structures. Struct Multidisc Optim. 2007;34(1):75–90.

[24] Bucalem ML, Bathe KJ. The Mechanics of Solids and Structures - Hierarchical Modeling and the Finite Element Solution. Springer; 2011.

[25] Bendsøe MP. Optimal shape design as a material distribution problem. Struct Optim. 1989;1(4):193–202.

[26] Ma ZD, Kikuchi N, Cheng HC. Topological design for vibrating structures. Comput Meth Appl Mech Eng. 1995;121(1-4):259–280.

[27] Fleury C, Braibant V. Structural optimization: A new dual method using mixed variables. Int J Numer Meth Eng. 1986;23:409–428.

Appendix

In this appendix, the detailed derivation of the sensitivity in Eq. (10) and the adjoint equations in Eq. (12) is outlined. First, the Lagrangian is formulated by adding the term composed of the adjoint variable $\tilde{\mathbf{u}}^T$ and the equations of state in Eq. (1) as follows:

$$\begin{aligned} L &= \mathbf{u}_{\text{input}}^T \mathbf{u}_{\text{input}} + \tilde{\mathbf{u}}^T (\mathbf{K} - \omega^2 \mathbf{M}) \mathbf{u} \\ &= \mathbf{u}^T \mathbf{H}^T \mathbf{H} \mathbf{u} + \tilde{\mathbf{u}}^T (\mathbf{K} - \omega^2 \mathbf{M}) \mathbf{u} \end{aligned} \tag{13}$$

Because the second term must always be zero, the Lagrangian must have the same value as the objective function. Thus, $f = L$. The derivative of the Lagrangian with respect to the i-th design variable d_i is obtained as follows:

$$\begin{aligned} \frac{\partial L}{\partial d_i} &= 2\mathbf{u}^T \mathbf{H}^T \mathbf{H} \frac{\partial \mathbf{u}}{\partial d_i} + \tilde{\mathbf{u}}^T (\mathbf{K} - \omega^2 \mathbf{M}) \frac{\partial \mathbf{u}}{\partial d_i} + \tilde{\mathbf{u}}^T \left(\frac{\partial \mathbf{K}}{\partial d_i} - \omega^2 \frac{\partial \mathbf{M}}{\partial d_i} \right) \mathbf{u} \\ &= \left\{ 2\mathbf{u}^T \mathbf{H}^T \mathbf{H} + \tilde{\mathbf{u}}^T (\mathbf{K} - \omega^2 \mathbf{M}) \right\} \frac{\partial \mathbf{u}}{\partial d_i} + \tilde{\mathbf{u}}^T \left(\frac{\partial \mathbf{K}}{\partial d_i} - \omega^2 \frac{\partial \mathbf{M}}{\partial d_i} \right) \mathbf{u} \end{aligned} \tag{14}$$

When the adjoint variable satisfies Eq. (12) the first term becomes zero and the sensitivity is obtained as Eq. (10).